Use of Side-Chain in Rational Design of N-Type Diketopyrrolopyrrole-based Conjugated Polymers: What did we find out?

Journal:	*Physical Chemistry Chemical Physics*
Manuscript ID:	CP-ART-05-2014-002322
Article Type:	Paper
Date Submitted by the Author:	27-May-2014

Complete List of Authors:	Patil, Satish; Indian Institute of Science, Solid State and Structural Chemistry Unit Kanimozhi, Catherine; Indian Institute of Science, Solid State and Structural Chemistry Unit Yaacobi-Gross, Nir; Imperial College London, Physics Burnett, Edmund; University of Massachusetts, Polymer Science and Engineering Briseno, Alejandro; University of Massachusetts, Polymer Science and Engineering Anthopoulos, Thomas; Imperial College London, Physics Salzner, Ulrike; Bilkent University, Chemistry

Use of Side-Chain in Rational Design of N-Type Diketopyrrolopyrrole-based Conjugated Polymers: What did we find out?

Catherine Kanimozhi,[a] Nir Yaacobi-Gross,[b] Edmund K. Burnett,[c] Alejandro L. Briseno,[c] Thomas D. Anthopoulos,[b] Ulrike Salzner[d] and Satish Patil[a]*

[a]Solid State and Structural Chemistry Unit, Indian Institute of Science, Bangalore 560012, India

[b]Department of Physics and Centre for Plastic Electronics, Blackett Laboratory, Imperial College London, London SW7 2BW, U.K.

[c]Department of Polymer Science and Engineering, University of Massachusetts, Amherst, Massachusetts 01003, United States

[d]Department of Chemistry, Bilkent University, 06800 Bilkent, Ankara, Turkey

To whom correspondence should be addressed

Dr. Satish Patil

Tel: +91-80- 22932651

Fax: +91-80-23601310

satish@sscu.iisc.ernet.in

Abstract:

The dominant role of substituted side chains in organic semiconductors is to increase the solubility in common organic solvents. In the recent past, many literature reports suggest that the side chains play a critical role in molecular packing and strongly impact charge transport properties of conjugated polymers. In this work, we have investigated the influence of side-chains on the charge transport behavior of a novel class of diketopyrrolopyrrole (**DPP**) based alternating copolymers. To investigate the role of side-chains, we prepared four diketopyrrolopyrrole-diketopyrrolopyrrole (**DPP-DPP**) conjugated polymers with varied side-chains and carried out a systematic study of thin film microstructure and charge transport properties in polymer thin-film transistors (**PTFT**). Combining results obtained from grazing incidence X-ray diffraction (GIXD) and charge transport properties in PTFTs, we conclude side-chains have a strong influence on molecular packing, thin film microstructure, and the charge carrier mobility of **DPP-DPP** copolymers. However, the influence of side-chains on optical properties was moderate. The preferential "*edge-on*" packing and dominant *n*-channel behavior with exceptionally high field-effect electron mobility values of >1 $cm^2V^{-1}s^{-1}$ were observed by incorporating hydrophilic (triethylene glycol) and hydrophobic side-chains of alternate units of the DPP. In contrast, moderate electron and hole mobilities were observed by incorporation of branched hydrophobic side-chains. This work clearly demonstrates that the subtle balance between hydrophobicity and hydrophilicity induced by side-chains is a powerful strategy to alter the molecular packing and improve the ambipolar charge transport properties in **DPP-DPP** based conjugated polymers. Theoretical analysis supports the conclusion that the side-chains influence polymer properties through morphology changes as there is no effect on the electronic properties in the gas phase. The exceptional electron mobility is at least partially caused through the strong intramolecular conjugation of the donor and acceptor as evidenced by the unusually wide conduction band of the polymer.

Introduction

Charge transport properties of π-conjugated polymers are affected by many factors: regioregularity, molecular weight, crystallinity, nature of the alkyl chains, and fabrication of thin film in electronic devices. The length and branching of side-chains has been found to have a profound impact on charge transport behaviour.[1] Traditionally, side-chains were introduced to impart solubility in π-conjugated polymers.[2-5] The increased solubility of polymers improves the processability of thin films in common organic solvents and leads to high degree of polymerization during the synthesis of polymers.[6,7] In the recent past, tremendous effort has been made to understand the role of side-chains on molecular packing and charge-carrier transport properties of π-conjugated polymers in thin-film transistors.[8,9] The side-chain engineering has guided synthetic chemists to design new materials with exceptionally high charge-carrier mobilities. Carrier mobilities of ~10 $cm^2V^{-1}s^{-1}$ have been achieved in *p*-type polymer thin-film transistors (**PTFTs)** for solution processable conjugated polymers.[10] However, air stable high mobility *n*-type organic semiconductors are rare which prevents the practical application of flexible electronics to ambipolar transistors, complementary circuits, and organic photovoltaic devices.[11]

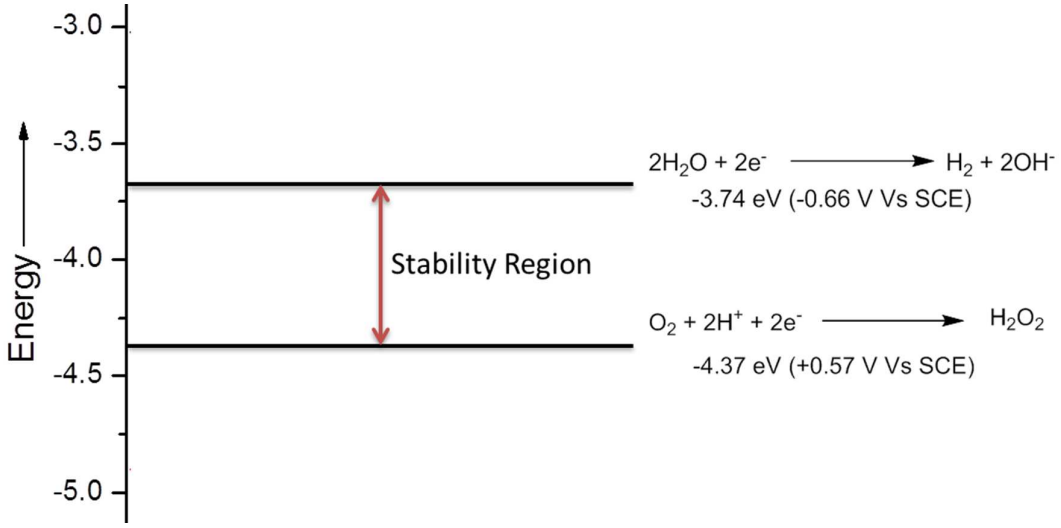

Figure 1: Electrochemical stability window of *n*-type semiconductors

Such uneven development of *p*-type semiconductors compared to *n*-type semiconductors shows the high sensitivity and low stability of these materials. This is

due to the serious drawbacks, including stability of the anions towards atmospheric oxygen and water.[12,13] Even though the factors governing the stability of *n*-type materials are not well understood yet, the first redox potential (E_{red1}) of the *n*-type semiconductor can be related to its capability to operate in ambient conditions.[14]

According to the de Leeuw's hypothesis,[15] the first reduction potential of *n*-type semiconductor should be greater than -0.66 V *vs* SCE (which is the reduction potential of H_2O) in order to avoid the oxidation of reduced anions by H_2O as shown in Figure 1. While a reduction potential greater than +0.57 V *vs* SCE would be required to prevent the oxidation of polymeric anions by oxygen. In experimental conditions, however, significant over potentials (0.5 V) are expected; therefore positive electrode potential is required for the electrochemical stability of *n*-type materials under ambient conditions.

This relationship has been further supported by the observation that the *n*-channel organic thin-film transistors (**OTFT)** devices recover their activity when re-measured under vacuum, after ambient exposure.[16] In view of these facts, it is surprising to observe *n*-channel **OTFTs** at ambient conditions. However, through appropriate synthetic routes and rational molecular design, several *n*-type molecular and polymeric semiconductors have been synthesized exhibiting **OTFT** electron mobilities of 0.1–2.0 $cm^2V^{-1}s^{-1}$ under inert/nitrogen atmosphere as well as at ambient atmosphere.[16-20]

By satisfying de Leeuw's hypothesis, our group has reported high electron mobility of 3 $cm^2V^{-1}s^{-1}$ for diketopyrrolopyrrole-diketopyrrolopyrrole based conjugated polymer.[21] The polymer was substituted with hydrophobic and hydrophilic side-chains on alternate units of DPP. The observation of such high electron mobility is striking, although we rationally coupled DPP to DPP to place LUMO energy deep to enhance the stability of anion towards water and oxygen. To understand the origin of high electron mobility, molecular packing and role of side-chains on the intermolecular interactions and polymer electrical properties in **OTFTs,** in the present work, we have designed and synthesized three new **DPP-DPP** copolymers bearing side chains with varying chain lengths and hydrophobic/hydrophilic groups. Significant efforts were also devoted to understand the role of side-chains on solution processability, molecular packing and thin film microstructure. Chemical structures of copolymers **2DPP-**OD-TEG, **2DPP-**OD-HE, 2**DPP-**OD-EH and **2DPP-**OD-OD are shown in Figure 2.

Our design principle for the synthesis of **DPP-DPP** copolymers with different alkyl/ethylene glycol side-chains serves to gain deeper insight into the role of alkyl chains on the lactam unit of DPP with a broader objective of understanding the basic relationship between structural features and performance characteristics of the newly synthesized polymers. The bulkier alkyl chain could result in larger twist angle and less planar geometry resulting in unfavourable steric interactions with adjacent conjugated subunits and leads to poor electronic communication between the donor and acceptor units,[22] which in turn can affect the intramolecular[23] charge transfer along the conjugated backbone.[24] This understanding can be effectively utilized to identify and modify the inherent properties of the molecular semiconductors in terms of its spectral width, band gap, thin film morphology and processing conditions. The important outcome from this study is the ambipolar charge transport and influence of hydrophilic chains on charge transport properties of **DPP-DPP** based copolymers.

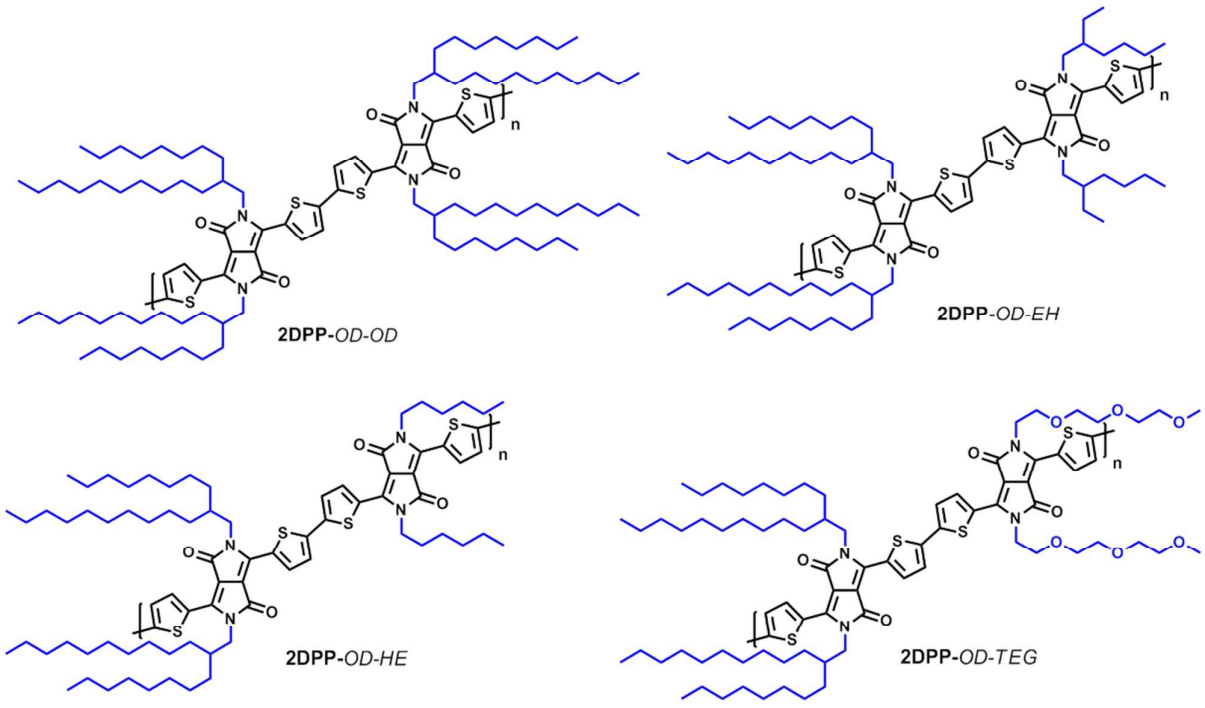

Figure 2: Chemical structure of DPP-DPP copolymers

Results and Discussions

Synthesis and Characterization

The synthetic route for the monomers and copolymers is outlined in Scheme 1 and 2. Compounds 1a-d and monomers **M1-M5** were synthesized by analogous procedures reported in the literature.[25,26] A detailed description of the synthesis of monomers is given in supporting information (SI). The key monomer **M1** was prepared from lithium diisopropylamide (LDA) and 2-isopropoxy-4,4,5,5-tetramethyl-1,3,2-dioxaboralane with small modifications in the literature procedure. All the monomers were obtained in good yield, purified by column chromatography and characterized by ^{1}H, ^{13}C NMR and elemental analysis. The **DPP-DPP** copolymers were synthesized via palladium-catalyzed Suzuki cross-coupling reactions between 3,6-bis(5-(4,4,5,5-tetramethyl-1,3,2-dioxaborolan-2-yl)thiophen-2-yl)-*N,N*-bis(2-octyldodecyl)-1,4dioxopyrrolo[3,4-c]pyrrole (**M1**) and 3,6-bis(5-bromothiophen-2-yl)-*N,N*-dialkyl-1,4-dioxopyrrolo[3,4-c]pyrrole (**M2-M5**). The polymerization reaction was carried out in the presence of a metal precursor catalyst $Pd_2(dba)_3$ and an active ligand tri(*o*-tolyl) phosphine (P(*o*-tol)$_3$). After completion of the polymerization, solvent was removed and the polymers were purified by precipitation in acetone and followed by Soxhlet extraction with methanol, acetone and hexane.

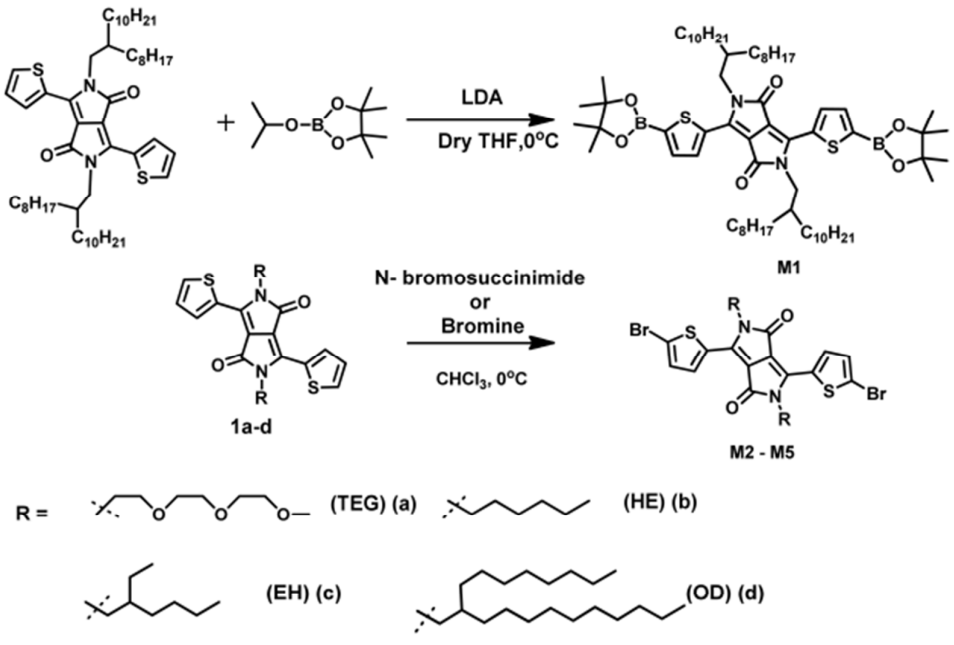

Scheme 1: Synthetic pathway for the monomers M1-M5.

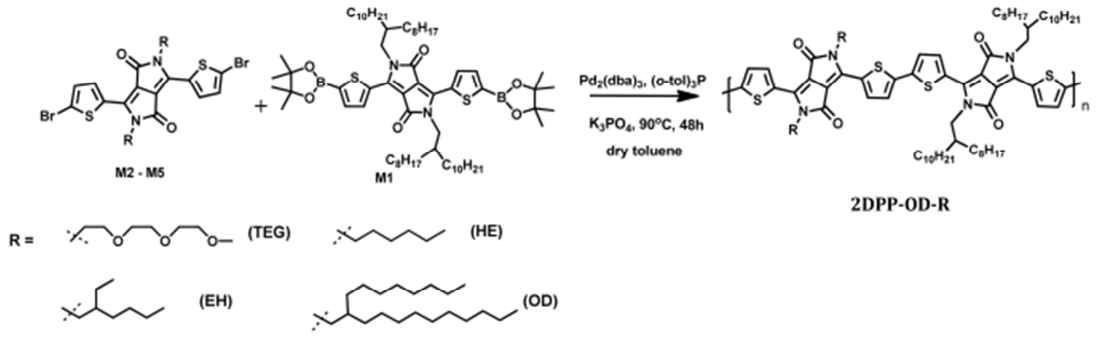

Scheme 2: Synthesis of DPP-DPP copolymers by Suzuki coupling reaction

GPC analysis of the copolymers was carried out in different solvents at elevated temperature. The average molecular weights (M_w and M_n) and polydispersity index (PDI) were obtained against a polystyrene standard and the results are summarized in Table 1. The results obtained from GPC analysis showed unusually high polydispersity and bimodal distribution. The low solubility of polymers in common organic solvents leads to aggregation at room temperature, which severely affects the polydispersity of conjugated polymers. Similar aggregation behavior has been observed in many **DPP** based conjugated polymers even at high temperatures.[27-29]

Electronic Structure and Optical Properties

The copolymers designed in this work with the **DPP-DPP** as a strong electron-deficient unit along the polymer chain exhibit unique optical and electronic properties. The optical absorption spectra of **2DPP-**OD-TEG, **2DPP-**OD-HE, 2**DPP-**OD-EH and **2DPP-**OD-OD in chloroform and in thin film are shown in Figure 3 and significant optical properties are summarized in Table 1. The absorption spectra of these copolymers in solution and in thin film exhibit a vibronically structured band with an onset at 1000 nm. The spectrum shows typical characteristics of homopolymers rather than alternating *donor-acceptor* copolymers. The striking difference noted in this family of **DPP-DPP** polymers are the huge red shift > 300 nm and high oscillator strength of the low energy band with exceptionally high molar extinction coefficient, while the intensity of the band observed at 400 nm is very low. The high oscillator strength and red shift of the low energy band suggests a longer conjugation length caused by the strong intermolecular interactions of the *donor-acceptor* repeating unit of polymer backbone that was enhanced by an increased degree of coplanarity. Such

enhanced intramolecular charge transfer in low band-gap polymers and oligomers have been found to improve the charge carrier mobility in OTFT.[30,31] Optical band-gap (E_g^{opt}) of these copolymers were estimated by extrapolating the onset of absorption edge and found to be ~1.2 eV. The thin film absorption spectra of **2DPP-**OD-TEG, **2DPP-**OD-HE, 2**DPP-**OD-EH and **2DPP-**OD-OD exhibit dramatic red shift of 46 nm, 15 nm, 24 nm and 22 nm respectively, suggesting the type of alkyl chain has a strong influence on conformational changes of the polymer backbone which leads to strong intermolecular interactions in the solid state.

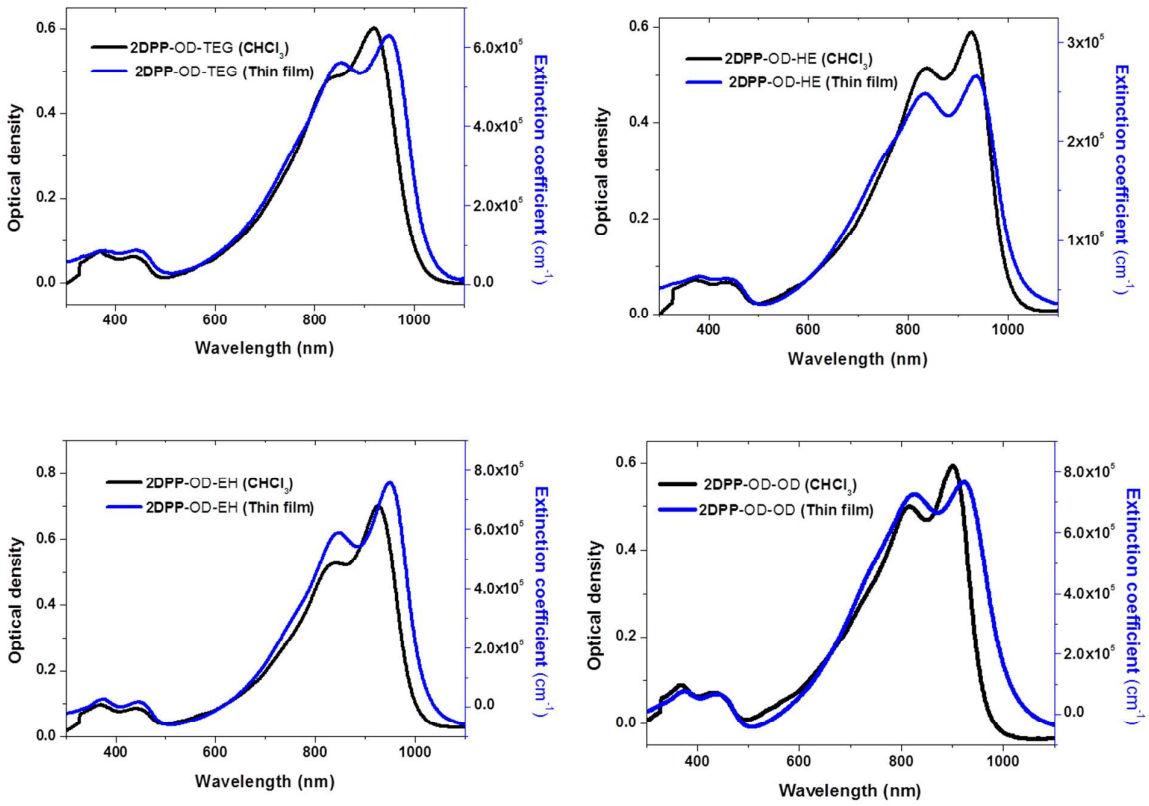

Figure 3: UV-Visible absorption spectra of DPP-DPP copolymers in chloroform and in thin film.

Table 1: Optical properties and Molecular weights of DPP-DPP polymers

	UV-Vis Absorption				Molecular weight data[a]		
Polymer	Solution	Thin Film			M_n	M_w	PDI
	λ_{max} (nm)	λ_{max} (nm)	λ_{onset} (nm)	E_g^{opt} (eV)	Kg/mol	Kg/mol	Mw/Mn
2DPP-OD-HE	924	939	1020	1.21	13.2	93.2	7.07
2DPP-OD-EH	924	948	1025	1.20	13.3	100.2	7.53
2DPP-OD-OD	898	920	1010	1.22	20.8	25.5	1.32
2DPP-OD-TEG	905	951	1023	1.21	67.3	314.0	4.66

[a]Determined by SEC in Trichlorobenzene and in chloroform based on polystyrene standards. The molecular weight for 2DPPOD-TEG is also reported in Reference 21.

The redox potentials and the HOMO-LUMO energy levels of the polymers have been determined electrochemically by cyclic voltammetry (CV) and the data is given in supporting information (Figure SI 2 and Table SI 1). All the four polymers show remarkable stability during reduction cycle of CV. The representative CV of multiple cycles for 2DPPOD-TEG is given in supporting information (Figure SI 3). The introduction of electron deficient DPP-DPP unit in the polymer backbone stabilizes the anion introduced during electrochemical reaction. In addition to that, the LUMO levels of conjugated polymers drastically shifts to deeper values as compared to conventional DPP-based copolymers such as DPP-benzothiadiazole and DPP-thienothiophene. This suggests that the strong overlap of *donor-acceptor* unit in coplanar fashion can bring substantial changes in energy levels, electrochemical and optical properties.

Thermal Properties

The thermal stability of these copolymers was investigated by thermal gravimetric analysis (**TGA**) and the data is given in SI. The thermal stability of molecular semiconductors is an important parameter. Thin films are often exposed to harsh environments during device fabrication such as thermal annealing during the evaporation of top electrode. TGA analysis of the copolymers indicates stability above 350°C with a decomposition temperature observed in the range of 360-380 °C (Figure SI 1).

Thin Film Morphology

The thin film morphology and roughness of the semiconductor layer is critical in improving the performance of OTFTs and OPVs. A large donor-acceptor interface is

required to ensure efficient charge dissociation, while trap free percolating pathways are essential to allow efficient charge transport. It is necessary to control the morphology of the active layer by various processing methods such as thermal and solvent annealing, or using mixed solvent systems. The nature of the polymer backbone and alkyl chains also has great influence on the morphology of the polymer thin film. Atomic force microscopy (AFM) and field emission scanning electron microscopy (FESEM) were employed to evaluate the thin film surface morphology of the copolymers.

AFM images of the copolymers spin coated or drop-casted from *o*-dichlorobenzene are shown in Figure 4. Prior to a deposition, the polymer solutions were sonicated and then passed through a membrane filter (pore diameter of 0.2 μm). Copolymers with linear, branched and hydropbobic/hydrophilic side-chains (**2DPP**-OD-HE, **2DPP**-OD-EH and **2DPP-**OD-TEG) results into fibrillar morphology made of nanofibers. In contrast, the copolymer with branched 2-octyldodecyl chains (**2DPP**-OD-OD) lacks fiber like features. The variation of the length and nature of side-chains results in a clear transition of well-defined fiber like structures to featureless morphology. This clearly indicates the strong influence of side chains on polymer conformations. Association of strong intermolecular interactions such as van der Waals, π-π stacking and difference in solubility are evident from the formation of structural morphology.

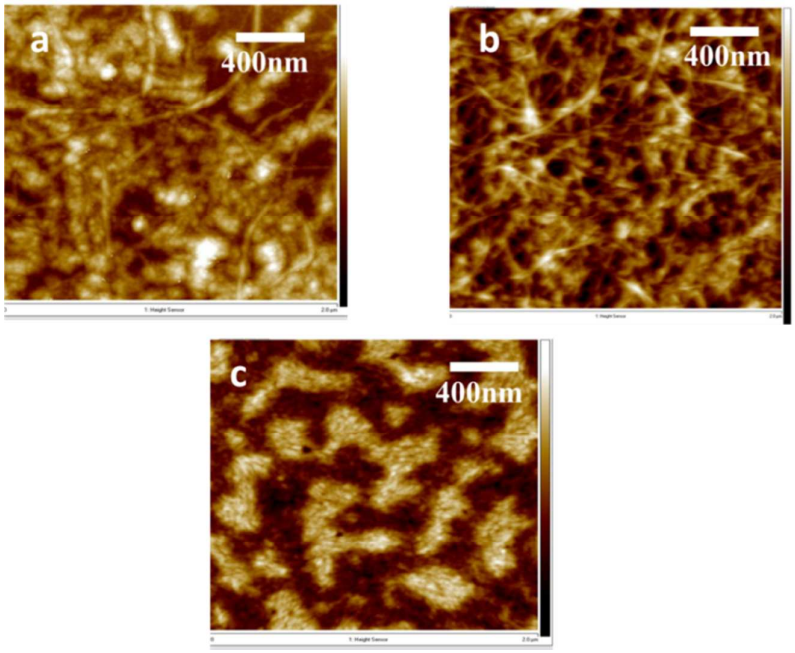

Figure 4: AFM height images of (a) 2DPP-OD-HE**, (b) 2DPP-**OD-EH **(c) 2DPP-**OD-TEG **spin coated from o-dichlorobenzene**

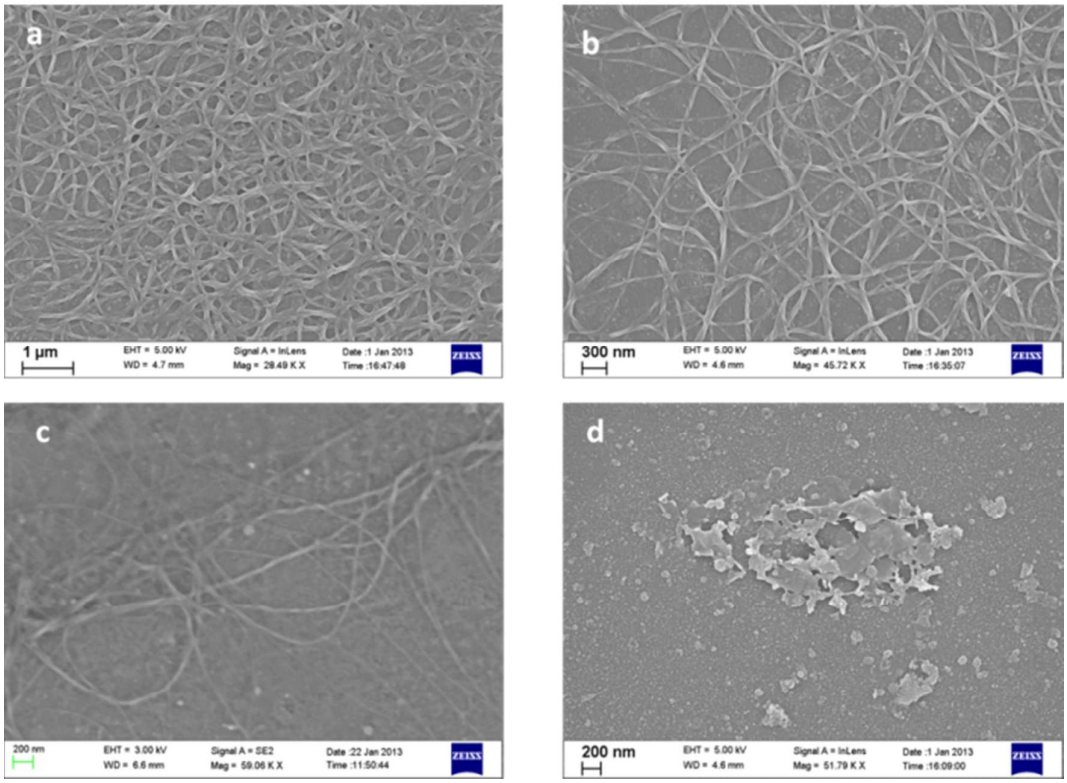

Figure 5: FESEM images of (a) 2DPP-OD-HE **(b) 2DPP-**OD-EH **(C) 2DPP-**OD-TEG **and (d) 2DPP-**OD-OD **drop casted from ODCB**

FESEM images of the copolymers were obtained from *o*-dichlorobenzene (**ODCB**) as shown in Figure 5. As observed in AFM images of the polymers similar nanofibrillar morphology was observed for copolymers **2DPP-**OD-TEG, **2DPP-**OD-HE, and 2**DPP-**OD-EH when casted from ODCB. Dispersed and entangled features of nanofibers were observed for **2DPP-**OD-HE, and 2**DPP-**OD-EH. In contrast, **2DPP-**OD-TEG exhibit long range nanofibrils structures with improved alignment. The width of nanofibers varies with diameter of 40-100 nm as we change the nature and length of side-chains. 2DPP-OD-TEG exhibits nanofibers with a diameter of 40 nm, whereas 2DPP-OD-HE and 2DPP-OD-EH shows nano fibres with a diameter of 100 and ~ 130 nm respectively. We have not observed fibrillar like morphology for 2DPP-OD-OD. These results clearly suggest hydrophilic triethylene glycol side chains promote the reorganization of polymer chains in more ordered aggregates and such structures have been proven beneficial for charge carrier transport with improved device performance. Unlike the polymers with linear hydrophobic/hydrophilic chains or smaller branched

chains, polymer with longer branched alkyl chains (**2DPP-**OD-OD) show no structures, instead resulted in thin film as shown in Figure 5 (d). The fibrillar morphology of polymers with short and linear alkyl chain clearly indicates the association of favorable intermolecular forces presents in the bulk polymer film and indeed the insulating alkyl chains affect the solid state packing of DPP-based conjugated polymer.

Thin Film X-ray Diffraction Studies

The effect of side chains on the thin film microstructures and the orientation of polymer crystallites on substrates was investigated by wide angle X-ray diffraction (XRD). The thin films of copolymers were casted from chlorobenzene on silicon substrates. The copolymers 2**DPP**-OD-HE and 2**DPP**-OD-TEG (Figure 6) with linear alkyl chains exhibit intense low angle Bragg peaks at $2\theta = 4.35^{o}$ attributed to the lamellar packing with an intermolecular distance of 20.2 Å and peak at $2\theta = 22^{o}$ corresponds to the π-π stacking interactions between the polymer conjugated planar backbones with a *d*-spacing in the order of 4.0 Å.

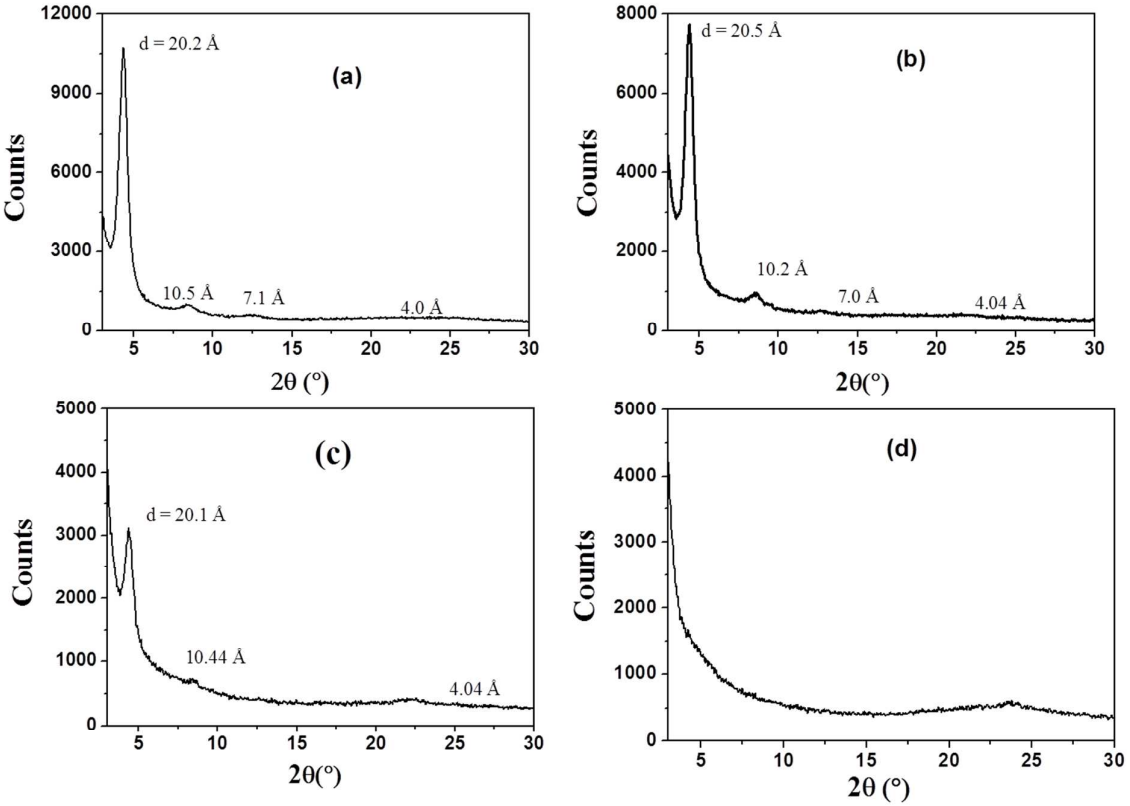

Figure 6: Thin film X-ray diffraction of DPP-DPP copolymers (a) 2DPP-OD-TEG **(b) 2DPP-**OD-HE **(c) 2DPP**-OD-EH **(d) 2DPP**-OD-OD **on a Si substrate**

Copolymers with branched alkyl chains such as **2DPP**-OD-EH and **2DPP**-OD-OD show reduced crystallinity or amorphous nature. Copolymer **2DPP**-OD-OD with repetitive dodecyl alkyl chains did not show small angle peaks, implying longer branched dodecyl alkyl chains prevent strong solid state packing.

Although the wide angle XRD is a powerful tool to probe the overall crystallinity of macromolecules, it is difficult to identify the mixed phases present in the thin film and the molecular packing of conjugated polymers, especially in the out-of-plane (q_z) and in-plane (q_{xy}) directions of the polymer backbone. These are crucial for charge transport properties in PTFT. We carried out grazing-incidence X-ray diffraction (**GIXD**) experiments to extract the orientation of the polymer crystallites by casting polymer thin films on Si substrates.

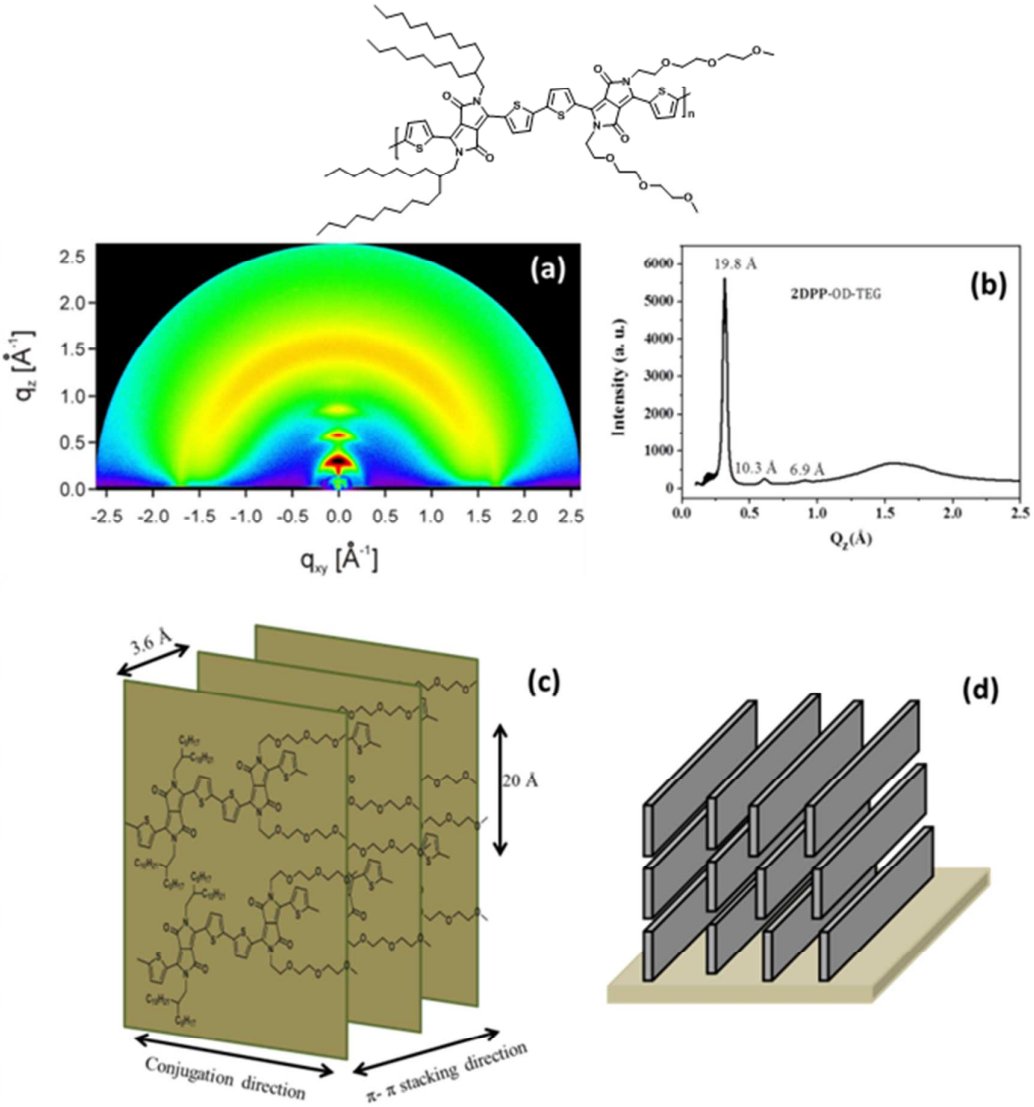

Figure 7: (a) GIXD pattern (b) intensity profile (c) schematic for possible orientation of polymer chains and (d) edge-on orientation of as-spun 2DPP-OD-TEG **thin films. Figure 7a adapted from reference 21 with permission from ACS.**

Figure 7 shows the scattering data and the intensity profile for as spun **2DPP-**OD-TEG. The high order lamellar structures (h00) parallel to the normal of the surface are clearly evident. A lamellar *d*-spacing of 20 Å was determined from the first-order (100) peak, which has a coherence length of 91 Å. Similarly an in-plane π-π stacking (010) peak associated with a *d*-spacing of 3.6 Å and a coherence length of 34 Å has been observed. The schematic (Figure 7 c, d) shows the packing of **2DPP-**OD-TEG and possible charge transport pathways such as the planar conjugated backbone direction and the π-π stacking direction. It shows that the polymer adopt an *edge-on* orientation on the substrate where the π-π stacking direction is parallel to the substrate. The shorter π-π stacking distance (3.6 Å) and large coherence length (34 Å) of π-π stacking interactions is attributed to the strong intermolecular interactions of the neighboring polymer chains and the presence of larger polymer crystallites with long range lattice ordering. Enhanced transport properties are expected for such films exhibiting long range order and films with short π-π stacking distance.

GIXD experiments were performed to understand the influence of solubilizing chains in DPP polymers on the resultant thin film morphology. Figure 8a shows the GIXD pattern and correspond line cuts of **2DPP-**OD-HE spin coated onto Si substrates. The diffractogram shows that the diffractions align vertically along the (h00) Bragg peaks, which display a lamellar texture that adopt an *edge-on* orientation. The reflections associated with the π-π stacking are most intense along the Q_{xy} plane, which shows that the orientation of this stacking is mostly parallel to the substrate. The lamellae (h00) are associated with a *d*-spacing of 20 Å (Figure 8a), the in-plane π-π stacking (010) peak has a *d*-spacing of 3.6 Å. Branching is introduced in **2DPP**-OD-EH with 2-ethyl hexyl chains, and Figure 8b shows branching increases the misalignment of the polymer, as a significant arching of these peaks can be seen, indicating that the crystallites are no longer completely aligned perpendicular to the substrate, but more randomly oriented. Figure 8c shows a thin film of **2DPP**-OD-OD which exhibits a dual texture of *face-on* and *edge-on* alignment as the (h00) reflection shows both out-of-plane and in-plane orientation.

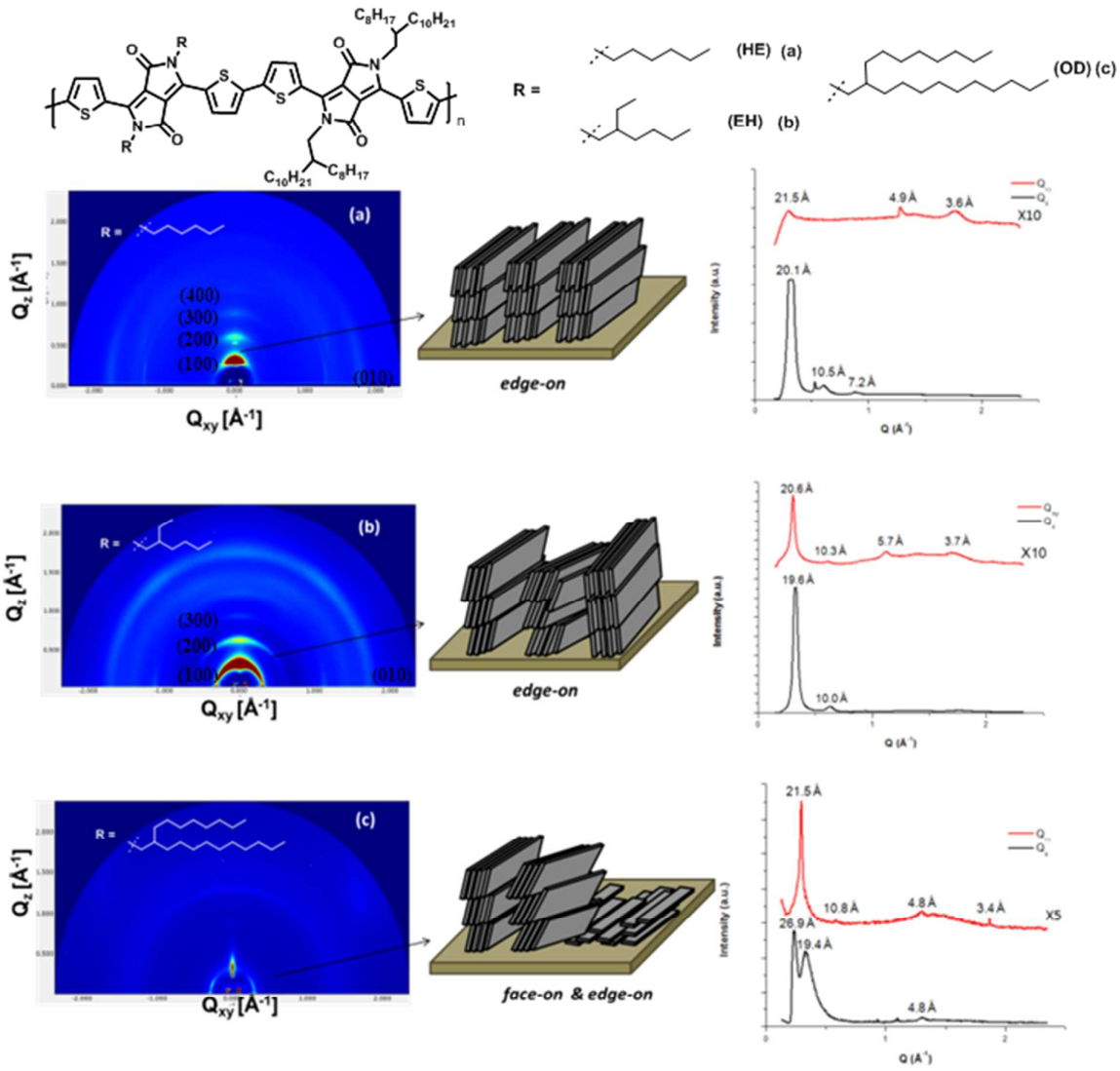

Figure 8: GIXD pattern and intensity profiles of as-spun 2DPP-OD-HE **(a) 2DPP-**OD-EH **(b) and 2DPP-**OD-OD **(c) thin films**

Density Functional Theory (DFT) Calculations

Electronic structure and molecular geometry were investigated with density functional theory (DFT). Monomers through tetramers of the DPP were optimized at the B3LYP/6-31G* level of theory. Octadecyl side groups were replaced with methyl groups. For the R group (compare scheme 1), TEG and methyl groups were tested. Because no differences between electronic structures of oligomers with TEG and methyl side-groups were found, all further calculations were done with methyl groups. The side-chains do not influence the electronic properties in the gas phase, confirms that the effects of different substituents occur through morphology changes. UV-

spectra were calculated with time-dependent DFT at TDB3LYP/6-31G*. All calculations were done with Gaussian 09.[32]

The oligomers are planar even in the gas phase, allowing for optimal conjugation along the chain. The four highest occupied and the four lowest unoccupied molecular orbitals of 4DPP are shown in Figure SI4. In spite of the (thiophene) donor and (DPP) acceptor character, the electron density in HOMO and LUMO is delocalized over donor and acceptor units. Only a slight tendency towards localization is observed for the lower lying occupied orbitals. This is in contrast to benzothiadiazole (BDT) copolymers where the LUMO is mainly localized on the BDT units.[33] As a result of the delocalized nature of orbitals, valence and conduction bands of the polymer, obtained by extrapolation of the band edges (Figure 9) are both wide. In stark contrast to copolymers containing BDT, the conduction band is wider than the valence band.[34] Thus, theory predicts higher intramolecular electron than hole mobility, in agreement with the experimentally observed high ambipolar mobility in OFETs.

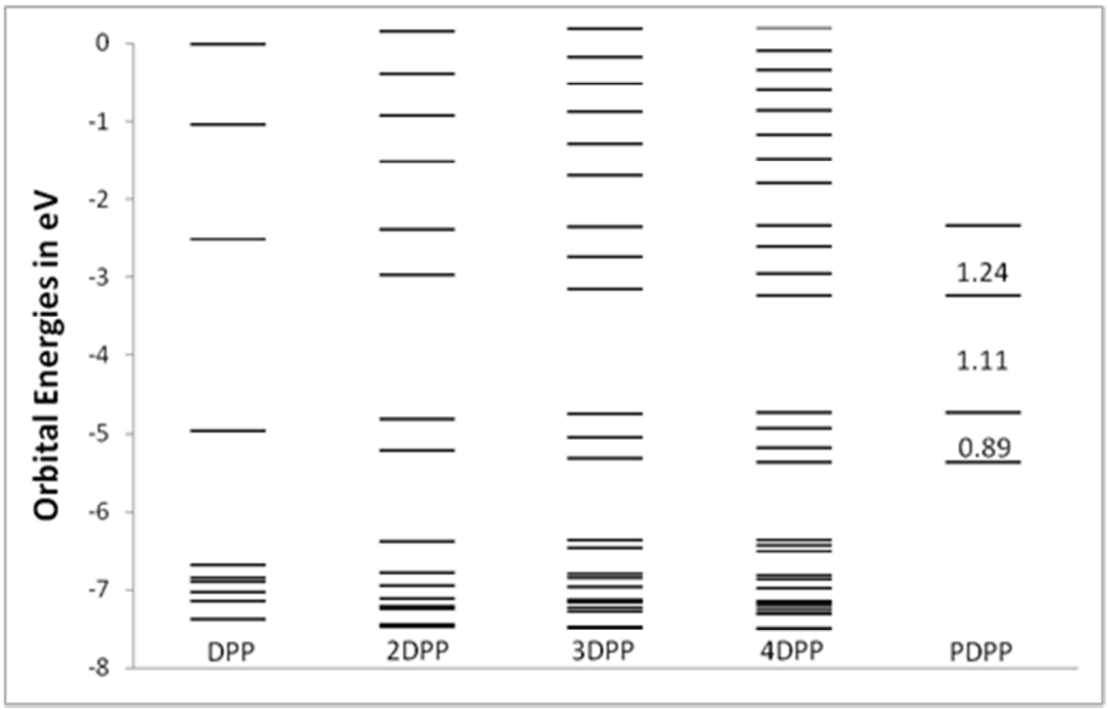

Figure 9: Orbital energies of 1DPP-4DPP and bands of PDPP.

Charges in the individual thiophene and DPP rings were evaluated with NBO analysis. In the ground state, DPP units are negatively charged with -0.15 e, reflecting the donor-acceptor character of the system. Upon excitation, however, the charge decreases to -0.14 e. Thus, there is practically no charge transfer upon excitation and

the small charge transfer that does occur, shifts electron density from DPP to thiophene. As a result, the low energy band does not have charge transfer character, it is rather a π–π* transition similar in nature to those in homopolymers. This is again in contrast to BDT copolymers where a charge transfer of 0.16 e from thiophene to BDT occurs upon excitation.

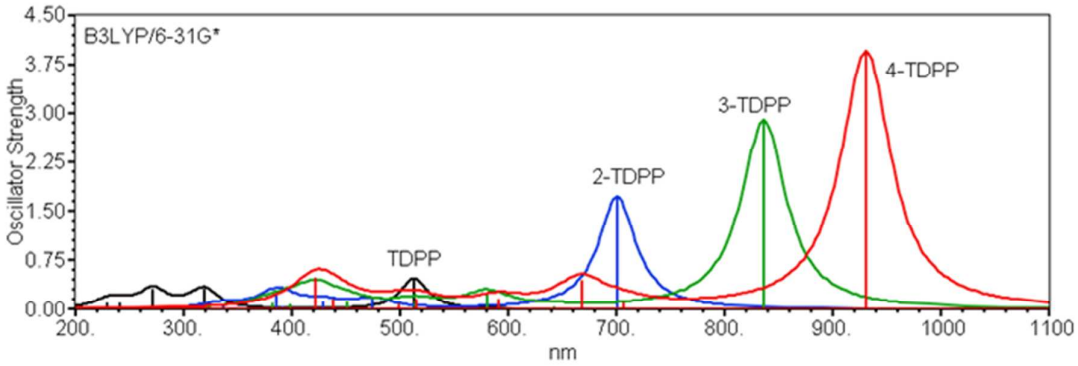

Figure 10. UV-spectra of 1DPP-4DPP at B3LYP/6-31G*

The electronic spectra of 1DPP-4DPP in Figure 10 demonstrate that there is a strong red-shift accompanied by a large increase in oscillator strength upon chain length extension. This is evidence for strong conjugation along the polymer backbone. The weak absorptions at higher energy are red-shifted, but change very little in intensity upon chain length increase. Analysis of the electron configurations contributing to the bands reveals that the strong low energy absorption is a HOMO-LUMO π–π* transition and the higher energy absorptions involve HOMO-1 through HOMO-3 and LUMO+1 through LUMO+3 just like in homopolymers.

In summary, theoretical analysis reveals that DPP-DPP copolymers differ significantly from their BDT analogues although the LUMO of DPP lies only 0.05 eV higher in energy than that of BDT. All theoretical and experimental results agree that DPP copolymers behave more like homopolymers with a single, strong, low-energy absorption. The exceptional electron mobility in this system is a result of the strong interaction between donor and acceptor in ground and excited states that is reflected in the wide conduction band and the large red-shift and high oscillator strength of the low-energy absorption.

Organic Field-Effect Transistor Measurements

The copolymers were tested using (1) bottom-gate bottom-contact (**BG-BC**) and (2) top-gate bottom-contact (**TG-BC**) transistor configurations. **BG-BC** devices were

made from Si/SiO_2 substrates with pre-patterned Au source/drain electrodes. The surface of SiO_2 was treated with hexamethyldisilazane (**HMDS**) in order to passivate its surface and prevent formation of charge trapping states. The polymer semiconductor layer was spun on top of the substrates to complete the transistor fabrication followed by thermal annealing at 140°C in nitrogen. **TG-BC** transistors were fabricated onto glass substrates containing pre-patterned Al source/drain electrodes.[35] The semiconducting polymer solution was then spun-cast onto the substrates at room temperature in nitrogen atmosphere. Following, the insulating fluoropolymer **CYTOP** (Ashai Glass) was sequentially spin casted directly onto the semiconducting polymer at room temperature followed by annealing at 100 ℃ for 5 minutes. Device fabrication was completed with the evaporation of the Al gate electrodes by thermal evaporation under high vacuum (10^{-6} mbar).

BG-BC transistor based on **2DPP-**OD-TEG exhibits clear ambipolar characteristics (Figure 11) with electron and hole mobilities in the order of $10^{-2}cm^2V^{-1}s^{-1}$. The extracted device parameters are summarized in Table 2. Charge carrier mobility in the saturated operating regime was extracted using Equation (1)

$$I_{DS} = \frac{W}{L}\frac{\mu_{FE}C_{ox}}{2}(V_G - V_t)^2 \qquad (1)$$

where, I_{DS} is the source-drain current, V_G is the applied gate voltage, V_t is the threshold voltage of the device, W is the channel width, L is the channel length, C_{ox} is the capacitance of the oxide layer and μ_{FE} is the field-effect mobility. The threshold voltage was extracted from the transfer characteristics measured with $V_D = |60\ V|$ and from the intersection of the extrapolated linear part of the $I_{DS}^{1/2}$ with the V_G axis. The on/off ratio for the transistors was also calculated yielding values in the order of 10^4.

Figure 12 displays the output and transfer characteristics of **BG-BC** transistors based on **2DPP**-OD-HE and **2DPP**-OD-EH copolymers. Unfortunately, no measurable channel current was obtained from transistors based on **2DPP**-OD-OD. On the other hand transistors based on the **2DPP**-OD-HE and **2DPP**-OD-EH copolymers show clear transistor action exhibiting hole mobility in the order of $10^{-4}cm^2V^{-1}s^{-1}$. Although similar charge carrier mobilities are obtained from the two polymers incorporating *n*-hexyl and 2-ethyl hexyl side chains, a large difference in the threshold of the two types of devices can be observed - V_{th}~ -15V and V_{th}~ -27 V for **2DPP**-OD-HE and **2DPP**-OD-EH based transistors, respectively. Since V_{th} is a measure of charge trapping sites present at the dielectric/polymer interface (i.e.

the semiconducting channel), the difference in the V_{th} most likely indicates the presence of a larger concentration of traps in the case of **2DPP**-OD-EH devices possibly due to branching which introduces increase structural, and hence energetic, disorder in the solid film as compared to devices based on **2DPP**-OD-HE. The polymer with triethylene glycol chains (**2DPP-**OD-TEG), on the other hand, shows low V_{th} and higher charge carrier mobility (Table 2).

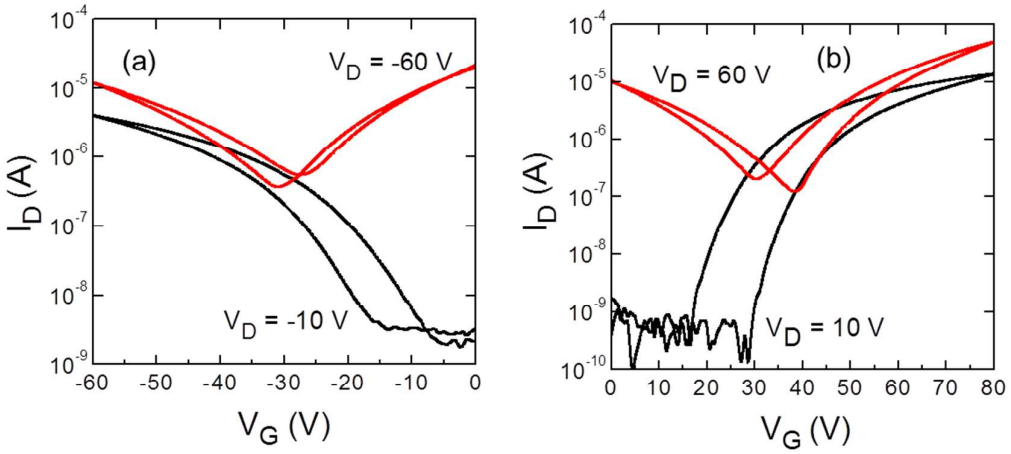

Figure 11: Transfer characteristics obtained at negative V_D (a) and positive V_D (b) from a BG-BC transistors based on the 2DPP-OD-TEG polymer

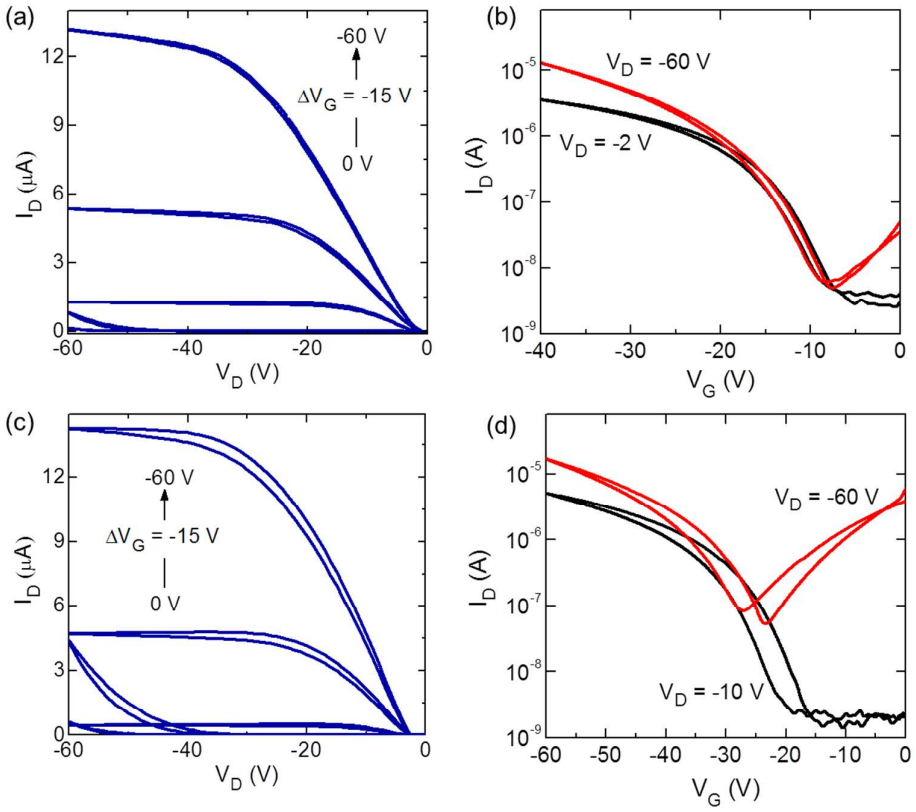

Figure 12: Output and transfer characteristics measured from BG-BC transistors based on the copolymer 2DPP-OD-HE **[(a) and (b), respectively] and the 2DPP-**OD-EH **copolymer [(c) and (b), respectively].**

Figure 13 displays a representative set of the transfer characteristics obtained from a TG-BC transistor based on the **2DPP-**OD-TEG copolymer. The devices show high channel currents as a direct result of the high electron mobility which for some devices exceeds 2 (±0.5) cm^2/Vs. The channel current on/off ratio is also high and typically in the order of 10^4 or higher. The reason for this dramatically enhanced electron mobility is believed to be the extended π-conjugation in combination with the long range structural order (lamellar packing) evidence for the latter is provided from the **GIXS** measurements. This unique combination of excellent intramolecular and intermolecular transport in the solid film leads to a dramatically enhanced electron mobility, as compared to the other copolymers. All four polymers were tested in **TG-BC** architecture. Unfortunately, only devices based on the **2DPP**-OD-TEG polymer, showed transistor function with the rest of the polymers resulting to non-functioning transistors i.e. typically devices exhibit high gate leakage currents, most likely due to non-optimized morphology of the polymer/dielectric interface.

In the case of the **TG-BC** transistors based on the **2DPP-**OD-TEG copolymer, the low work function Al (4.3 eV) source-drain electrode was replaced with the high work function gold (Au ~5 eV) electrodes. As evaporated Au electrodes were treated with the contact work function modifier pentafluorobenzene (**PFBT**). A very interesting observation is that as opposed to the **BG-BC** transistors characteristics shown in Figure 11, **TG-BC** devices show no hole transporting characteristics (Figure 14) and exhibit clear unipolar electron transport character even when the source/drain electrodes are replaced with the high work function and hence the hole injecting Au electrodes.

Table 2: Summary of OFET device characteristics

Polymer	Device Configuration	G/S	Gate Dielectric	μ_e ($cm^2V^{-1}s^{-1}$)	μ_h ($cm^2V^{-1}s^{-1}$)	I_{on}/I_{off}	V_{th} (V)
2DPPOD-HE	**BG-BC**	**Au**	**SiO_2**	**-**	**8×10^{-4}**	**10^3**	**-15.2**
2DPPOD-EH	**BG-BC**	**Au**	**SiO_2**	**-**	**7×10^{-4}**	**10^3**	**-27.2**
2DPPOD-OD	**BG-BC**	**Au**	**SiO_2**	**-**	**-**	**-**	**-**
2DPPOD-TEG	**BG-BC**	**Au**	**SiO_2**	**10^{-2}**	**10^{-2}**	**10^4**	**<± 10**
2DPPOD-TEG	**TG-BC**	**Al**	**CYTOP**	**>2**	**-**	**10^4**	**2**

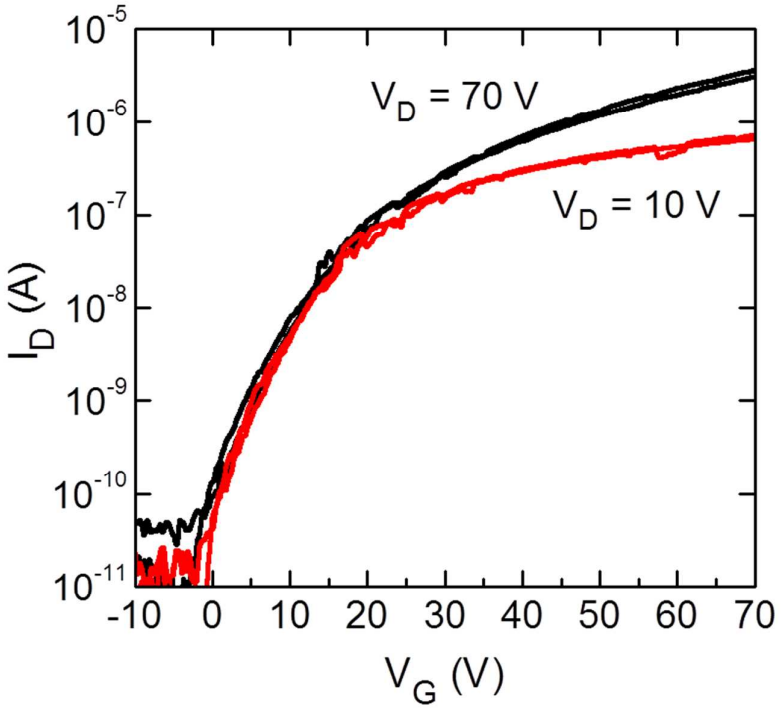

Figure 13: Transfer characteristics measured from a TG-BC transistor based on the 2DPP-OD-TEG copolymer. Adapted (From reference 21) with permission from American Chemical Society.

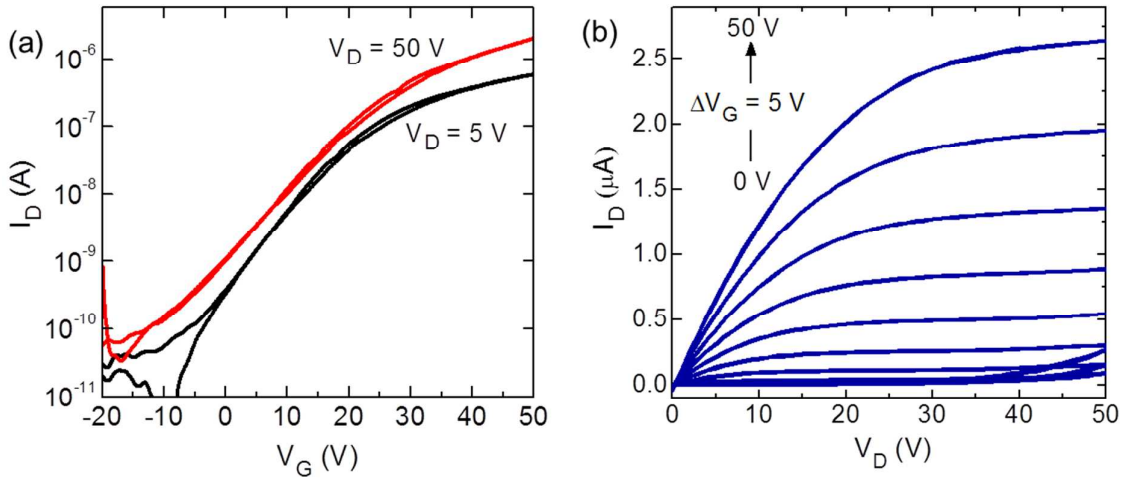

Figure 14: Transfer (a) and output (b) characteristics measured for TG-BC transistors based on 2DPP-OD-TEG

Summary and Conclusions

In summary, we have developed a novel series of alternating copolymers by coupling electron-deficient DPP-based monomers. The coupling of diketopyrrolopyrrole with diketopyrrolopyrrole in an alternate fashion affords remarkable improvement in optical properties and ambipolar charge carrier mobility. In this contribution, we also emphasized the critical role of substituted alkyl chains on the charge transport properties, thin film morphology, and electronic properties of these newly developed molecular semiconductors. The results obtained suggests that a better electronic structure or the position of LUMO energy is not only a decisive factor for improving charge carrier mobility but also the superior morphology of the polymer thin films and the conformation induced by substituted side chains contributes significantly to the solid state packing and the charge transport. The electronic structure, thin film morphology, and molecular packing obtained from GIXD measurements presents a detailed understanding of charge transport properties of this emerging class of molecular semiconductors. The novel synthetic design approach and demonstration of organic field-effect transistors (**2DPP-**OD-TEG*)* with electron mobilities >2 $cm^2V^{-1}s^{-1}$ will further validate the potential of **DPP**-based conjugated polymers. We also make a note that molecular weight has a strong influence on charge carrier mobilities of these polymers.

Acknowledgements: The authors acknowledge financial support from the Department of Science and Technology, India through the Indo-UK Apex Program and Ministry of Communication and Information Technology under a grant for the Centre of Excellence in Nanoelectronics, Phase II. E. K. B and A. L. B acknowledge the National Science Foundation for their support (DMR-1112455). GIXD was carried outat Stanford Synchrotron Light Source (SSRL).

References

(1) Choi, D.; Jeong, B.-S.; Ahn, B.; Chung, D. S.; Lim, K.; Kim, S. H.; Park, S. U.; Ree, M.; Ko, J.; Park, C. E. *ACS Appl. Mater.Interfaces* **2011**, *4*, 702.

(2) Postema, A. R.; Liou, K.; Wudl, F.; Smith, P. *Macromolecules* **1990**, *23*, 1842.

(3) Luo, J.; Liu, S.; Haller, M.; Liu, L.; Ma, H.; Jen, A. K. Y. *Adv. Mater.* **2002**, *14*, 1763.

(4) Hotta, S.; Rughooputh, S. D. D. V.; Heeger, A. J.; Wudl, F. *Macromolecules* **1987**, *20*, 212.

(5) Jen, K.-Y.; Miller, G. G.; Elsenbaumer, R. L. *J. Chem. Soc., Chem. Commun.* **1986**, 1346.

(6) Wu, P.-T.; Xin, H.; Kim, F. S.; Ren, G.; Jenekhe, S. A. *Macromolecules* **2009**, *42*, 8817.

(7) Guo, X.; Kim, F. S.; Jenekhe, S. A.; Watson, M. D. *J. Am. Chem. Soc.* **2009**, *131*, 7206.

(8) Sariciftci, N. S.; Smilowitz, L.; Heeger, A. J.; Wudl, F. *Science* **1992**, *258*, 1474.

(9) Chen, J.; Cao, Y. *Acc. Chem. Res.* **2009**, *42*, 1709.

(10) Li, J.; Zhao, Y.; Tan, H. S.; Guo, Y.; Di, C.-A.; Yu, G.; Liu, Y.; Lin, M.; Lim, S. H.; Zhou, Y.; Su, H.; Ong, B. S. *Sci. Rep.* **2012**, *2*.

(11) Eder, F.; Klauk, H.; Halik, M.; Zschieschang, U.; Schmid, G.; Dehm, C. *Appl. Phys. Lett.* **2004**, *84*, 2673.

(12) Chua, L.-L.; Zaumseil, J.; Chang, J.-F.; Ou, E. C. W.; Ho, P. K. H.; Sirringhaus, H.; Friend, R. H. *Nature* **2005**, *434*, 194.

(13) Murphy, A. R.; Fréchet, J. M. J. *Chem. Rev.* **2007**, *107*, 1066.

(14) Usta, H.; Risko, C.; Wang, Z.; Huang, H.; Deliomeroglu, M. K.; Zhukhovitskiy, A.; Facchetti, A.; Marks, T. J. *J. Am. Chem. Soc.* **2009**, *131*, 5586.

(15) de Leeuw, D. M.; Simenon, M. M. J.; Brown, A. R.; Einerhand, R. E. F. *Synth. Met.* **1997**, *87*, 53.

(16) Newman, C. R.; Frisbie, C. D.; da Silva Filho, D. A.; Brédas, J.-L.; Ewbank, P. C.; Mann, K. R. *Chem. Mater.* **2004**, *16*, 4436.

(17) Kim, C.; Facchetti, A.; Marks, T. J. *Science* **2007**, *318*, 76.

(18) Lei, T.; Dou, J.-H.; Cao, X.-Y.; Wang, J.-Y.; Pei, J. *J. Am. Chem. Soc.* **2013**, *135*, 12168.

(19) Zhao, Y.; Guo, Y.; Liu, Y. *Adv. Mater.* **2013**, *25*, 5372.

(20) Nielsen, C. B.; Turbiez, M.; McCulloch, I. *Adv. Mater.* **2013**, *25*, 1859.

(21) Kanimozhi, C.; Yaacobi-Gross, N.; Chou, K. W.; Amassian, A.; Anthopoulos, T. D.; Patil, S. *J. Am. Chem. Soc.* **2012**, *134*, 16532.

(22) Naik, M. A.; Venkatramaiah, N.; Kanimozhi, C.; Patil, S. *J. Phys. Chem. C.* **2012**, *116*, 26128.

(23) Dimitrakopoulos, C. D.; Malenfant, P. R. L. *Adv. Mater.* **2002**, *14*, 99.

(24) Mayer, A. C.; Toney, M. F.; Scully, S. R.; Rivnay, J.; Brabec, C. J.; Scharber, M.; Koppe, M.; Heeney, M.; McCulloch, I.; McGehee, M. D. *Adv. Funct. Mater.* **2009**, *19*, 1173.

(25) Burckstummer, H.; Weissenstein, A.; Bialas, D.; Wurthner, F. *J. Org. Chem* **2011**, *76*, 2426.

(26) Huo, L.; Hou, J.; Chen, H.-Y.; Zhang, S.; Jiang, Y.; Chen, T. L.; Yang, Y. *Macromolecules* **2009**, *42*, 6564.

(27) Li, W.; Roelofs, W. S. C.; Wienk, M. M.; Janssen, R. A. J. *J. Am. Chem. Soc.* **2012**, *134*, 13787.

(28) Bronstein, H.; Chen, Z.; Ashraf, R. S.; Zhang, W.; Du, J.; Durrant, J. R.; Shakya Tuladhar, P.; Song, K.; Watkins, S. E.; Geerts, Y.; Wienk, M. M.; Janssen, R. A. J.; Anthopoulos, T.; Sirringhaus, H.; Heeney, M.; McCulloch, I. *J. Am. Chem. Soc.* **2011**, *133*, 3272.

(29) Bijleveld, J. C.; Gevaerts, V. S.; Di Nuzzo, D.; Turbiez, M.; Mathijssen, S. G. J.; de Leeuw, D. M.; Wienk, M. M.; Janssen, R. A. J. *Adv. Mater.* **2010**, *22*, E242.

(30) Kim, Y. H.; Park, S. K.; Moon, D. G.; Kim, W. K.; Han, J. I. *Jpn. J. Appl. Phys.* **2004**, *43*, 3605.

(31) Ando, S.; Nishida, J.-i.; Tada, H.; Inoue, Y.; Tokito, S.; Yamashita, Y. *J. Am. Chem. Soc.* **2005**, *127*, 5336.

(32) Frisch, M. J. T., G. W.; Schlegel, H. B.; Scuseria, G. E.; Robb, M. A.; Cheeseman, J. R.; Scalmani, G.; Barone, V.; Mennucci, B.; Petersson, G. A.; Nakatsuji, H.; Caricato, M.; Hratchian, H. P.; Izmaylov, A. F.; Bloino, J.; Zheng, G.;

Sonneberg, J. L.; Hada, M.; Ehara, M.; Toyota, K.; Fukuda, R.; Hasegawa, J.; Ishida, M.; Nakajima, T.; Honda, Y.; Kitao, O.; Nakai, H.; Vreven, T.; Montgomery, J. A., Jr.; Peralta, J. E.; Ogliaro, F.; Bearpark, M.; Heyd, J. J.; Brothers, E.; Kudin, K. N.; Staroverov, V. N.; Kobayashi, R.; Normand, J.; Raghavachari, K.; Rendell, A.; Burant, J. C.; Iyengar, S. S.; Tomasi, J.; Cossi, M.; Rega, N.; Millam, J. M.; Klene, M.; Knox, J. E.; Cross, J. B.; Bakken, V.; Adamo, C.; Jaramillo, J.; Gomperts, R.; Stratmann, R. E.; Yazyev, O.; Austin, A. J.; Cammi, R.; Pomelli, C.; Ochterski, J. W.; Martin, R. L.; Morokuma, K.; Zakrzewski, V. G.; Voth, G. A.; Salvador, P.; Dannenberg, J. J.; Dapprich, S.; Daniels, A. D.; Farkas, O.; Foresman, J. B.; Ortiz, J. V.; Cioslowski, J.; Fox, D. J. *Gaussian 09, Revision A.1, Gaussian, Inc.: Wallinford, CT,* **2009**.

(33) Gibson, G. L.; McCormick, T. M.; Seferos, D. S. *J. Am. Chem. Soc.* **2011**, *134*, 539.

(34) Salzner, U.; Karaltı, O.; Durdağı, S. *J Mol Model* **2006**, *12*, 687.

(35) Smith, J.; Zhang, W.; Sougrat, R.; Zhao, K.; Li, R.; Cha, D.; Amassian, A.; Heeney, M.; McCulloch, I.; Anthopoulos, T. D. *Adv. Mater.* **2012**, *24*, 2441.

Electronic Supplementary Information (ESI) available: [Materials, Experimental details, additional spectra and device fabrication details are provided in supporting information.]. See DOI: 10.1039/b000000x/

Graphical Abstract:

In this work, we have investigated the influence of side-chains on the charge transport behavior of a novel class of diketopyrrolopyrrole (**DPP**) based alternating copolymers. To investigate the role of side-chains, we prepared four diketopyrrolopyrrole-diketopyrrolopyrrole (**DPP-DPP**) conjugated polymers with varied side-chains and carried out a systematic study of thin film microstructure and charge transport properties in polymer thin-film transistors (**PTFT**). Combining results obtained from grazing incidence X-ray diffraction (GIXD) and charge transport properties in PTFTs, we conclude side-chains have a strong influence on molecular packing, thin film microstructure, and the charge carrier mobility of **DPP-DPP** copolymers. However, the influence of side-chains on optical properties was moderate. The preferential "*edge-on*" packing and dominant *n*-channel behavior with exceptionally high field-effect electron mobility values of >1 $cm^2V^{-1}s^{-1}$ were observed by incorporating hydrophilic (triethylene glycol) and hydrophobic side-chains of alternate units of the DPP. In contrast, moderate electron and hole mobilities were observed by incorporation of branched hydrophobic side-chains. The exceptional electron mobility is at least partially caused through the strong intramolecular conjugation of the donor and acceptor as evidenced by the unusually wide conduction band of the polymer.